Article

Two Fe-Zr-B-Cu nanocrystalline magnetic alloys produced by mechanical alloying technique

Jason Daza [1], Wael Ben Mbarek [1], Lluisa Escoda [1], Joan Saurina [1], and Joan-Josep Suñol [1,*]

[1] Department of Physics, University of Girona, 17003 Girona, Spain
* Correspondence: joanjosep.sunyol@udg.edu

Abstract: Fe rich soft magnetic alloys are candidates for applications as magnetic sensors and actuators. These alloys can also be added to hard magnetic compounds to obtain spring magnets. In this work we produce two nanocrystalline Fe-Zr-B-Cu alloys by the powder metallurgy powder technology of mechanical alloying. The increase of the boron content favors the reduction of the crystalline size. Thermal analysis (by differential scanning calorimetry) shows at temperatures between 450 and 650 K wide exothermic processes, associated with the relaxation of tensions of the alloys produced by milling. At high temperatures, a main crystallization peak is found. The apparent activation of this process was determined by Kissinger and isoconversional methods. The values are compared with those found in the scientific literature. Likewise, adapted thermogravimetry permits to determine the Curie temperature. The functional response has been analyzed by hysteresis loop cycles. According to the composition, the decrease of the Fe/B ratio diminishes the magnetic soft behavior.

Keywords: mechanical alloying; thermal analysis; soft magnetic; Fe based.

1. Introduction

In magnetic alloys, it is important to check the thermal stability of the magnetic phase and their soft-hard behaviour. It is also known that the magnetic properties change if the alloy is amorphous or crystalline. Mechanical alloying is a production technique applied for the development of powdered Fe rich nanocrystalline alloys [1,2]. Mechanical alloying is a powder metallurgy technology applied before sintering or consolidation [3,4]. The thermal stability of these alloys front crystalline growth is determinant due to the loss of soft behaviour as increasing the crystallite size. A key parameter to determine this thermal stability is the apparent activation energy of crystallization [5,6].

Soft ferromagnetic alloys are characterized by low coercive field, H_c, high saturation magnetic flux density, B_s, and high permeability, μ [7]. Low coercivity and high permeability favours low core losses in applications under alternate current magnetic fields. Thus, the control of these parameters is associated to the optimization of the energy savings [8]. Regarding the saturation magnetic flux density, higher values favour the application in low dimensional systems, as the consequent miniaturization [9]. Likewise, the thermal behaviour of these alloys allows for the establishing of the working temperature limits; the Curie temperature that marks the transition from ferromagnetic to paramagnetic and the loss of soft magnetism. Magnetic thermogravimetry has been applied to determine this limiting temperature [10].

In the last decades, several families of nanocrystalline soft magnetic alloys have been developed as alternatives to traditional ferrites such as Finemet [11], Nanoperm [12], Hitperm [13] or Nanomet [14]. Figure 1 show the typical values of these nanocrystalline alloys representing the initial permeability as a function of the saturation magnetic flux density. For comparison, information about traditional ferrites, sendust, permalloy, Si steels, Fe-based amorphous and Co-based amorphous is also provided in this graph.

In this work, two nanocrystalline Fe-Zr-B-Cu Nanoperm-type alloys have been produced by mechanical alloying. The thermal stability has been determined by thermal analysis by checking the apparent activation energy of the main crystalline growth process and the Curie temperature.

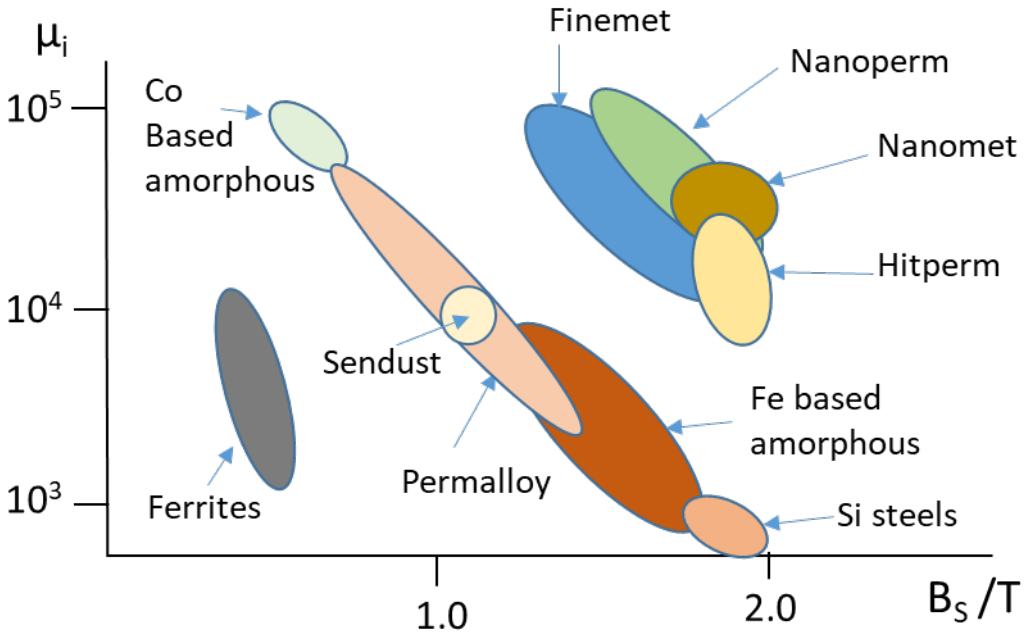

Figure 1. Permeability versus magnetic flux density of several families of soft magnetic alloys.

2. Materials and Methods.

In this work, two Fe rich soft magnetic alloys were produced by mechanical alloying (MA). The initial compositions were $Fe_{85}Zr_6B_8Cu_1$ (at.%) and $Fe_{80}Zr_5B_{13}Cu_1$ (at.%); both Nanoperm-type. These alloys are labelled as A and B respectively. The precursors were elemental Fe (6-8 μm, 99.9% purity), Zr (5 μm, 98 % purity), B (20 μm, 99.7% purity) and Cu (45 μm, 99 % purity) powders. The milling was performed in in a planetary ball mill device (Fritsch P7 model). The milling process was achieved up to 50 h, under argon atmosphere, with hardened steel vials and balls as milling media, a ball-to-powder weight ratio (BPR) of about 10:1, and a rotation speed of 700 r.p.m. To prevent an excess in the internal vial temperature the milling was performed in cycles (10 minutes on followed by 5 minutes off). The experimental conditions have been chosen to optimize the alloys production by the mechanical alloying technique.

The particles powder morphology and distribution size were checked by scanning electron microscopy (SEM) in a DSM960A Zeiss apparatus. The final composition of the alloys was checked by inductive coupled plasma (ICP) in a Liberty-RL ICP Varian equipment. The nanocrystalline state (bcc Fe rich phase) was confirmed by X-Ray diffraction (XRD) patterns collected using a D-500 Siemens (Bruker, Billerica, MA, USA) equipment with CuKα radiation (λ = 0.15406 nm). The thermal stability of the mechanically alloyed powders was studied by differential scanning calorimetry (DSC) using a LabSys Evo 1600°C apparatus. The DSC curves were measured in the temperature range of 350–950 K at different heating rates: 5, 10, 20, 30 and 40 K/min under argon flow (20 ml/min). The thermogravimetry measurements were performed in a TGA Star^e Mettler Toledo model under Ar atmosphere at a heating rate of 10 K/min. The magnetic parameters such as intrinsic coercivity, *Hc*, saturation magnetization, *Ms*, and saturation to remanence ratio, *Mr*/*Ms*, were determined by analysing the magnetic hysteresis loops collected in a Lakeshore 7404 vibrating sample magnetometer (VSM) at room temperature, under an applied magnetic field of 15 kOe.

3. Results

The alloys are produced in powder form. Figure 2 shows two micrographs of alloys A and B milled for 50 hours. The rounded shape with smooth contours of the particles and a micrometric size of these is verified. Also, a relatively wide distribution in particle sizes was found. In order to check the particle size and its distribution, the particle size of five micrographs of each sample have been measured. The results are shown in Figure 3.

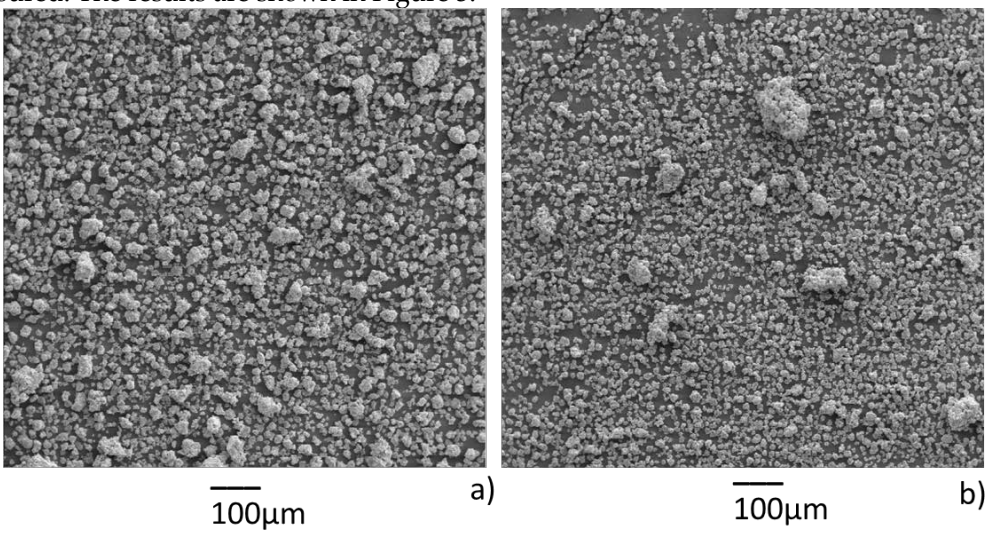

Figure 2. SEM micrographs of alloys A (left) and B (right) milled for 50 hours.

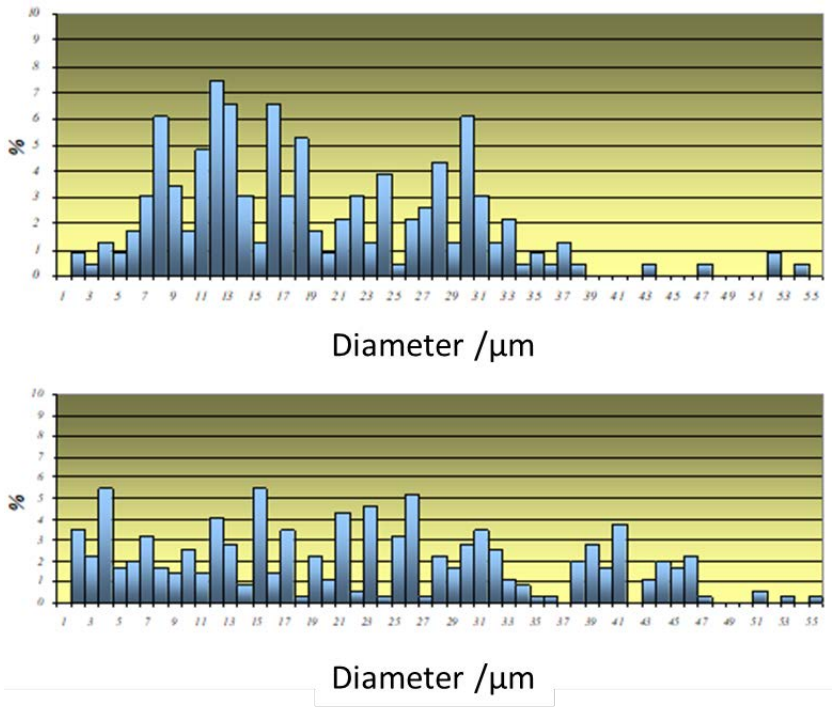

Figure 3. Particle size distribution of alloys A (up) and B (down) milled for 50 hours.

The contamination was measured by ICP. Mechanical alloying process favours contamination from the milling tools. Likewise, the high surface/volume ratio of the particles induces surface oxidation. Nevertheless, the results show only slight contamination from the milling tools (basically Fe from container and walls) and oxygen in both alloys after 50 h of milling. Similar results were previously reported [15]. ICP results show that the Fe content increase over the nominal composition was 1.7±0.3, and 1.6±0.4 at.% for alloys A and B, respectively. Likewise, the oxygen content was

2.1±0.6 and 1.9±0.5 at.% for alloys A and B, respectively; probably a decrease in the iron percentage is associated to a reduction in the oxygen level.

Regarding microstructural analysis, XRD patterns confirms the formation of the cubic bcc structure with nanocrystalline size. The analysis applying the Williamson-Hall method permits to determine both, the crystallite size and the microstrain. For alloy A. the crystalline size is 26 ± 2 nm and the microstrain 0.58 ± 0.06; whereas for alloy B the values are 15 ± 2 nm (crystalline size) and 0.61 ± 0.08 (microstrain). Thus, the increase of boron content favours the reduction of the crystalline size.

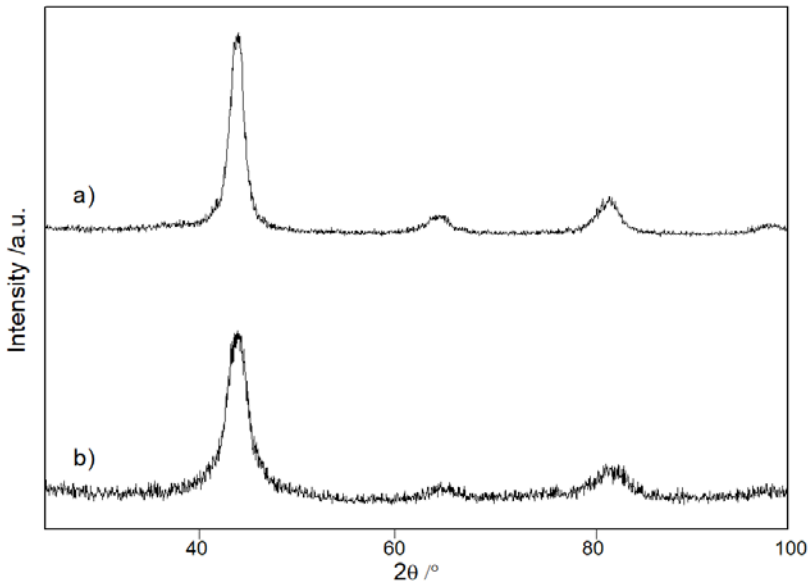

Figure 4. X-Ray diffraction pattern of alloys A (a) and B (b) milled for 50 hours.

Figure 5 shows the DSC curves of the two alloys milled for 50h (heating rate: 10K/min). The general shape of the curves is similar in both alloys. Around 400 K, a large exothermic process begins. This process is typically found in samples produced by mechanical alloying [16]. Its origin is the microstructural relaxation of the high density of crystallographic defects induced during grinding/milling. The existence of small exothermic processes of the same character at higher temperatures could be an indicator of a not completely homogeneous sample. The weak exothermic process around 750 or 780 K in both samples is typical of a partial recrystallization of the material. The main exothermic process (in the form of a peak, with temperatures around 850 and 880 K in each sample) is due to the crystalline growth of the Fe-rich bcc phase. The development of high performance soft magnetic alloys is associated to amorphous and low crystalline size nanocrystalline alloys. It is necessary that the crystallite size remains smaller than 10 nm. In this case, by applying the random anisotropy model, Hc depending on D^6 because the domain wall effect diminishes and each grain behaves as a single domain. Thus, crystalline growth should be avoided and the crystallization temperature is a limiting temperature for application of these alloys [17].

One of the most characteristic parameters to characterize a crystallization process is its activation energy. The apparent activation energy of the main crystallization process has been calculated by applying the Kissinger method [18], whose typical representation (for both analysed alloys) is shown in figure 6. This method is based on the determination of the peak temperature of the crystallization process in the experiments carried out at different heating rates. The values are 282 ± 26 and 299 ± 25 kJ/mol for alloys A and B respectively. These values are consistent with those of the crystallization of the bcc-Fe rich phase.

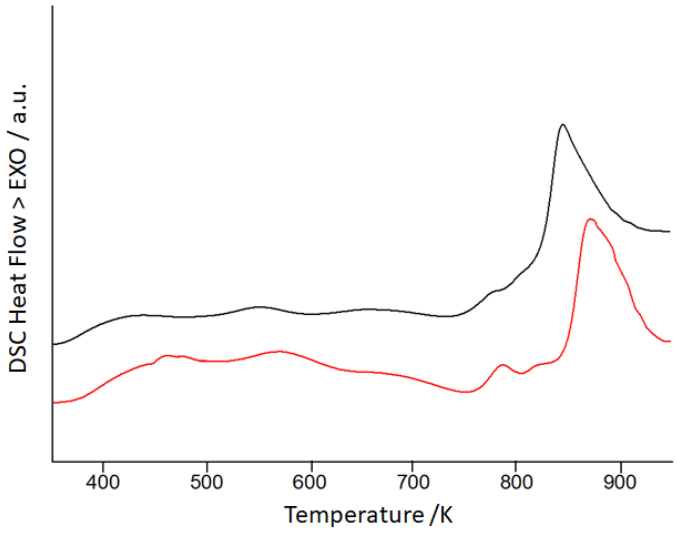

Figure 5. DSC scans at 10 K/min of the as milled alloys A (black) and B (red).

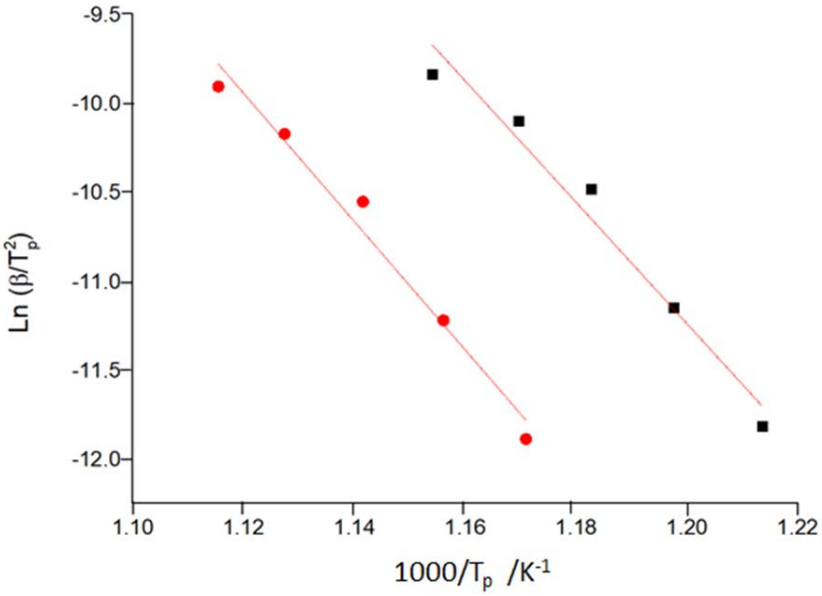

Figure 6. Kissinger plot of the as milled alloys A (black) and B (red).

The calculated energies of this work are compared with some of those of the scientific literature (applying Kissinger method) in table 1.

This work's values are in the same relatively wide range [19-25]. The shift in the activation energies can be related to different composition and microstructure (including crystallographic defects). This dispersion is also found in research of the sane alloy system. Liu et al. [26] found values ranged between 138 and 356 kJ/mol in Fe-Ni-Zr-B alloys produced by mechanical alloying.

Table 1. Apparent activation energy of the crystallization processes (Fe rich bcc phase).

Composition at.%	Activation energy kJ mol^{-1}	Initial structure	Reference
$Fe_{83}P_{16}Cu_1$	238	Amorphous	[19]
$Fe_{68}Nb_6B_{23}Mo_3$	310	Amorphous	[20]
$Fe_{80}Si_{20}$	245	Amorphous	[21]
$Fe_{83}P_{16}Cu_1$	219	Nanocrystalline	[22]
$Fe_{83}P_{14.5}Cu_1Al_{1.5}$	238	Nanocrystalline	[22]
$Fe_{78}Si_{11}B_9$	370	Amorphous	[23]
$Fe_{73.5}Cu_1B_7Si_{15.5}Nb_3$	295	Nanocrystalline	[23]
Fe (99.9% purity)	224	Nanocrystalline	[24]
$Fe_{71}Si_{16}B_9Cu_1Nb_3$	341	Amorphous	[25]
$Fe_{85}Zr_6B_8Cu_1$	282	Nanocrystalline	This work
$Fe_{80}Zr_5B_{13}Cu_1$	299	Nanocrystalline	This work

Likewise, there are other linear methods (normally based on the determination of the peak temperature). However, the activation energy was similar to those calculated by Kissinger, and the differences are based more on the linear relationships established between the parameters than on real differences in the crystallization process [20]. For example, it is not the same to represent $\ln(\beta/T_p^2)$ than $\ln(\beta/T_p)$ (in both cases as a function of the inverse of the peak temperature).

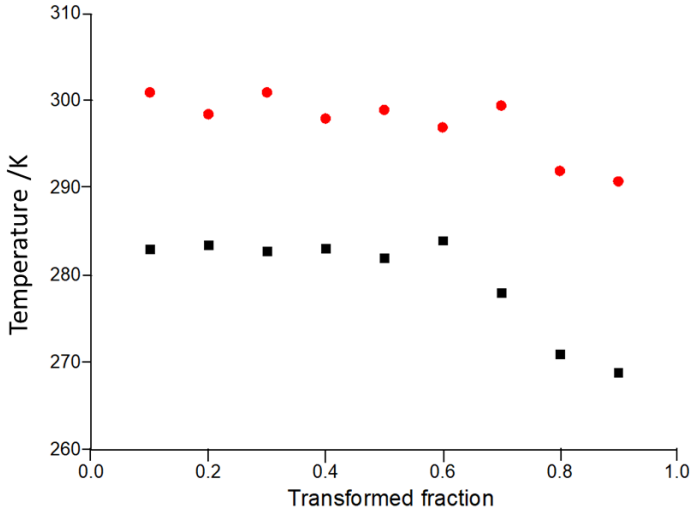

Figure 7. The activation energy as a function of the transformed fraction of the as milled alloys A (black) and B (red).

The scientific literature on the activation energy of crystallization processes shows methods in which two energies are determined: that of crystal nucleation and growth respectively [27], the second having a higher value. This approximation is not applicable when there is only crystal growth (for example in initially nanocrystalline alloys). In recent decades, a set of methods based on the calculation of the apparent activation energy has been extended to different transformation/crystallization fractions. These methods are defined as isoconversional [28-29]. Figure 7 shows the calculated values (for the main exothermic process) at fractions transformed from 0.1 to 0.9 [29]. A fairly stable value is found, except for high fractions where a slight decrease in activation energy is detected. In the zone of low-medium transformed fraction, the set of calculated values is similar to that determined by applying the Kissinger method, around 288 and 298 kJ/mol for alloys A and B, respectively. Being nanocrystalline alloys, it is normal for this value to be stable, since the

crystal nucleation process is negligible [30]. Thus, the activation energy is that corresponding to the crystal growth mechanism. At high transformed fractions, the degree of transformation slows down and the local activation energy decreases [31]. There is an impingement between the crystal grains.

Regarding the magnetic behaviour, one of the most characteristic and fundamental thermomagnetic parameters of magnetically soft alloys is the Curie temperature. Temperature that marks the maximum value of applicability (magnetic) of the alloy, since it defines the change from a ferromagnetic to a paramagnetic behaviour. The Curie temperature can be determined from the DSC curves [32]. However, in the case of overlapping processes (as is often the case with alloys produced by mechanical alloying) their determination can be complex [33]. Therefore, on many occasions this temperature is determined directly by magnetic measurements (of variation of magnetization as a function of temperature). Another alternative based on thermal analysis techniques is magnetic thermogravimetry. By adding a small external magnet near the sample zone and performing the thermogravimetry experiment, an apparent variation of the sample mass during the transition from ferromagnetism to paramagnetism is detected. This method, previously applied [34], has been used in the present study. Figure 8 shows the thermogravimetric curves recorded. A variation of the apparent mass of the samples around 937 and 971 K for alloys A and B, respectively, is found. These temperatures are typical of ferromagnetic alloys with a high iron content.

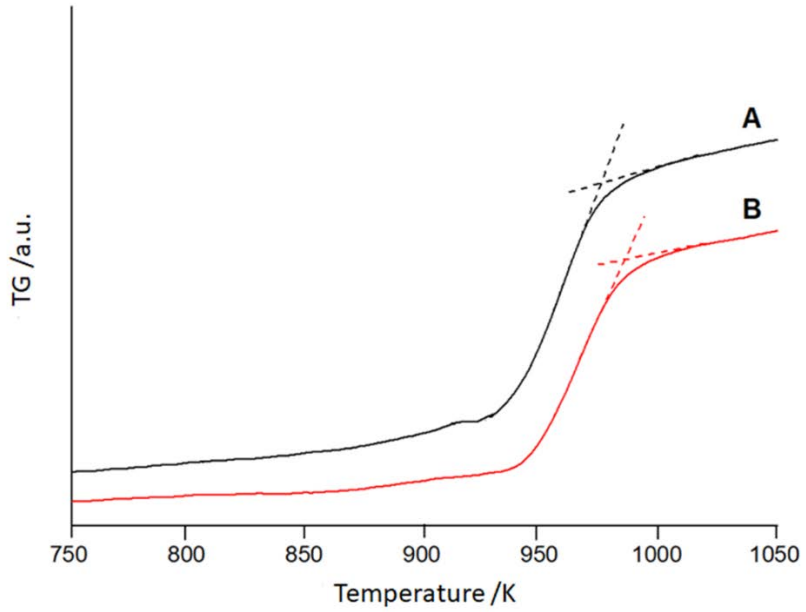

Figure 8. Magnetic thermogravimetry curves of alloys the as milled alloys A (black) and B (red).

As the interest of these alloys is based on their magnetic response, the hysteresis cycles of both alloys (after 50 h of milling) at room temperature have been obtained. Figure 9 shows both magnetic cycles (magnetization M as a function of external magnetic field H). Its analysis allows to determine the parameters that define its soft magnetic response. The determined values are shown in Table 2. Magnetization of saturation M_s 146 and 139 $A \cdot m^2 \cdot Kg^{-1}$, coercivity H_C $10.6 \cdot 10^{-4}$ T and 12.4 10^{-4} T and remanence 0.60 and 0.71 $A \cdot m^2 \cdot Kg^{-1}$ for alloys A and B respectively.

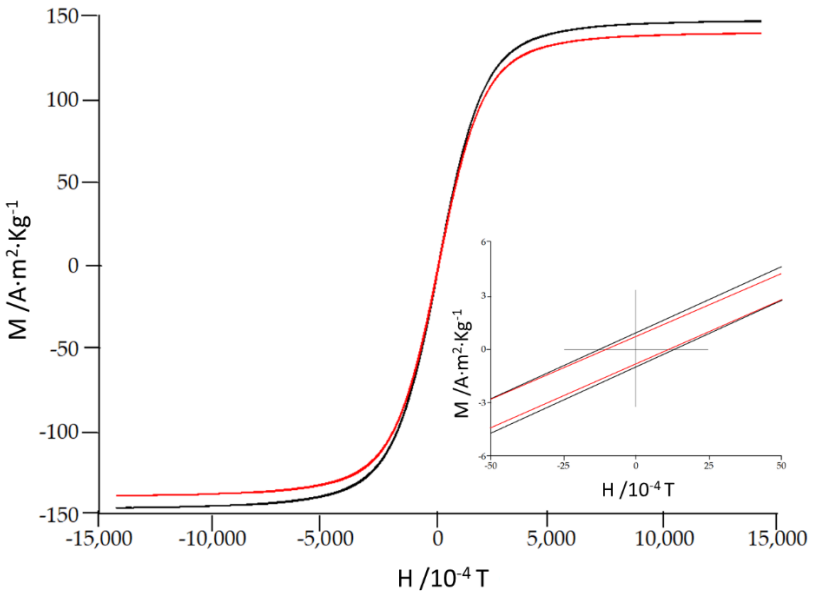

Figure 9. Magnetic hysteresis loops at room temperature of the as milled alloys A (black) and B (red). The inset corresponds to the (0,0) region.

Table 2. Magnetic parameters derived from hysteresis cycles at room temperature.

Alloy	H_c	M_s	M_r	M_r/M_s
	10^{-4} T	$A \cdot m^2 \cdot Kg^{-1}$	$A \cdot m^2 \cdot Kg^{-1}$	10^{-3}
$Fe_{85}Zr_6B_8Cu_1$	10.6	146	0.60	4
$Fe_{80}Zr_6B_{13}Cu_1$	12.4	139	0.71	5

The main influence will be related to the Fe atoms local environment and to Fe-Fe interatomic distance due to the magnetic behaviour of iron. For it, it was expected the detected diminution in the magnetization of saturation as decreasing the Fe/B ratio. Likewise, it is known that the magnetic properties depend strongly on the microstructure evolution, crystalline size, internal stress, particle shape anisotropy, magnetic anisotropy, and magnetostriction of the materials [35]. In our work, higher B content decreases crystallite size and this effect counteract partially (favouring soft behaviour) the effect of the reduction of the magnetic element, Fe. The other values of the magnetic properties are similar in both samples. The relatively low value of the squareness ratio is typical of alloys obtained in powder form by mechanical alloying [6].

Thus, we can conclude that the alloys produced are magnetically soft at room temperature and that thermal analysis is useful to determine the thermal stability (front crystallization and front magnetic transition) of this magnetic behaviour.

5. Conclusions

Two ferromagnetic nanocrystalline alloys of the Fe-Zr-B system have been produced by mechanical alloying (powder shape). Its thermal stability has been analysed using thermal analysis measurements. High apparent activation energy as well as high transition temperatures (crystallization, Curie) are needed to prevent the loss of the soft behaviour caused by the increase of the crystalline size or the ferro- to paramagnetic transition. The differential calorimetry allows to determine (by Kissinger and isoconversional methods) the apparent energy of activation of the main process of crystallization. Being the lowest value, 288 kJ/mol, the one corresponding to the alloy with

higher iron content. Regarding the transition temperatures, both the peak crystallization temperature and the Curie temperature are higher in the alloy with lower Fe/B ratio.

Regarding the magnetic response, the characteristic parameters are similar in both alloys, being the magnetization of saturation higher in the alloy with more iron content due to the Fe-Fe magnetic moment atomic interactions.

Author Contributions: Conceptualization, J-J.S.; methodology, J.S.; software, X.X.; formal analysis, W. B-M.; investigation, J.D; writing—original draft preparation, J.D. and J-J.S; supervision, L.E.

Funding: Financial support from PID2020-115215RB-C22 project.

Institutional Review Board Statement: Not applicable.

Informed Consent Statement: Not applicable.
Data Availability Statement: Data will be made available upon reasonable requests to the authors.

Conflicts of Interest: The authors declare no conflict of interest.

References

1. Gouasmia, T.; Loudjani, N.; Boulkra, M.; Benchiheub, M.; Belakroum, K.; Bououdina, M. Morphology, structural and microstructural characterizations of mechanically alloyed $Fe_{50}Co_{40}Ni_{10}$ powder mixture. *Applied Physics A - Science & Processing* **2022**, *128(10)*, 935. https://doi.org/10.1007/s00339-022-06074-y.
2. Panigrahi, M.; Avar, B. Influence of mechanical alloying on structural, thermal and magnetic properties of $Fe_{50}Ni_{10}Co_{10}Ti_{10}B_{20}$ high entropy soft magnetic alloy. *Journal of Materials Science - Materials in Electronics* **2021**, *32*, 21124-21134. https://doi.org/10.1007/s10854-021-06612-z.
3. Chaubey, A.K.; Konda Gokuldoss, P.; Wang, Z.; Scudino, S.; Mukhopadhyay, N.K.; Eckert, J. Effect of Particle Size on Microstructure and Mechanical Properties of Al-Based Composite Reinforced with 10 Vol.% Mechanically Alloyed Mg-7.4%Al Particles. *Technologies* **2016**, *4*, 37. https://doi.org/10.3390/technologies4040037.
4. Karthiselva, N.S.; Bakshi, S.R. Reactive Spark Plasma Sintering and Mechanical Properties of Zirconium Diboride–Titanium Diboride Ultrahigh Temperature Ceramic Solid Solutions. *Technologies* **2016**, *4*, 30. https://doi.org/10.3390/technologies4030030.
5. Chebli, A.; Cesnek, M.; Djekoun, A.; Suñol, J.J.; Niznansky, D. Synthesis, characterization and amorphization of mechanically alloyed $Fe_{75}Si_{12}Ti_6B_7$ and $Fe_{73}Si_{15}Ti_5B_7$ powders. *Journal of Materials Science* **2022**, *57(26)*, 12600-12615. https://doi.org/10.1007/s10853-022-07404-4.
6. Carrillo, A.; Daza, J.; Saurina, J.; Escoda, L.; Suñol, J.J. Structural, Thermal and Magnetic Analysis of $Fe_{75}Co_{10}Nb_6B_9$ and $Fe_{65}Co_{20}Nb_6B_9$ Nanostructured Alloys. *Materials* **2021**, *14(16)*, 4542. https://doi.org/10.3390/ma14164542.
7. Yao, K.F.; Shi, L.X.; Chen, S.Q.; Shao, Y.; Chen, N.; Jia, J.L. Research progress of Fe based soft magnetic amorphous/nanocrystalline alloys. *Acta Physica Sinica* **2018**, *58(1)*, 17-27. https://doi.org/10.7498/aps.67.20171473.
8. Zhu S.; Duan F.; Ni J.L.; Feng S.J.; Liu X.S.; Lv Q.R.; Kan X.C. Soft magnetic composites FeSiAl/MoS_2 with high magnetic permeability and low magnetic loss. Journal of Alloys and Compounds 2022, 926, 166893. https://doi.org/10.1016/j.jallcom.2022.166893.
9. Yamazaki, T.; Tomita, T.; Uji, K.; Kuwata, H.; Sano, K.; Oka, C.; Sakurai, J.; Hata, S. Combinatorial synthesis of nanocrystalline FeSiBPCuC-Ni-(Nb.;Mo) soft magnetic alloys with high corrosion resistance. *Journal of Non-Crystalline Solids* **2021**, *563*, 120808. https://doi.org/10.1016/j.jnoncrysol.2021.120808.
10. Miglierini, MB.; Dekan, J.; Cesnek, M.; Janotova, I.; Svev, P.; Budjos, M.; Kohout, J. Hyperfine interactions in Fe/Co-B-Sn amorphous alloys by Mossbauer spectrometry. *Journal of Magnetism and Magnetic Materials* **2020**, *500*, 6417. https://doi.org/10.1016/j.jmmm.2020.166417.
11. Zhao, M.; Pang, J.; Zhang, Y.R.; Zhang, W.; Xiang, Q.C.; Ren, Y.L.; Li, X.Y.; Qiu, K.Q. Optimization of crystallization, microstructure and soft magnetic properties of $(Fe_{0.83}B_{0.11}Si_{0.02}P_{0.03}C_{0.01})_{(99.5)}Cu_{0.5}$ alloy by rapid annealing. *Journal of Non-Crystalline Solids* **2022**, *579*, 121380. https://doi.org/10.1016/j.jnoncrysol.2021.121380.
12. Hasiak, M.; Laszcz, A.; Zak, A.; Kaleta, J. Microstructure and Magnetic Properties of NANOPERM-Type Soft Magnetic Material. *Acta Physica Polonica A* **2019**, *135(2)*, 284-287. https://doi.org/10.12693/APhysPolA.135.284.
13. Ozturk, S.; Icin, K.; Gencturk, M.; Gobuluk, M.; Svec, P. Effect of heat treatment process on the structural and soft magnetic properties of Fe38Co38Mo8B15Cu ribbons. *Journal of Non-Crystalline Solids* **2020**, *527*, 119745. https://doi.org/10.1016/j.jnoncrysol.2019.119745.
14. Nishiyama, N.; Tanimoto, K.; Makino, A. Outstanding efficiency in energy conversion for electric motors constructed by nanocrystalline soft Magnetic Nanomet cores. *AIP Advances* **2016**, *6*, 055925. https://doi.org/10.1063/1.4944341.

15. Suñol, J.J.; González, A.; Saurina, J.; Escoda, L.; Bruna, P. Thermal and structural characterization of Fe-Nb-B alloys prepared by mechanical alloying. *Materials Science and Engineering A* **2004**, *375-377*, 874-880. https://doi.org/10.1016/j.msea.2003.10.194.
16. Taghvaei, A.H.; Bednarcik, J.; Eckert, J. Influence of annealing on microstructure and magnetic properties of cobalt-based amorphous/nanocrystalline powders synthesized by mechanical alloying. *Journal of Alloys and Compounds* **2015**, *632*, 296-302. https://dx.doi.org/10.1016/j.jallcom.2015.01.180.
17. Daza, J.; Ben Mbarek, W.; Escoda, L.; Suñol, J.J. Characterization and analysis of nanocrystalline soft Magnetic alloys: Fe based. *Metals* **2021**, *11(12)*, 1896. https://doi.org/10.3390/met11121896.
18. Vyazovkin, S. Kissinger Method in Kinetics of Materials: Things to Beware and Be Aware of. *Molecules* **2020**, *25(12)*, 2813. https://doi.org/10.3390/molecules25122813.
19. Chen, F.G.; Wang, Y.G.; Mian, X.F.; Hong H.; Bi, K. Nanocrystalline $Fe_{83}P_{16}Cu_1$ soft magnetic alloy produced by crystallization of its amorphous precursor. Journal of Alloys and Compounds 2013, 549, 26-29. https://dx.doi.org/10.1016/j.jalcom.2012.09.072.
20. Liu, Y.; Zhu, M.; Du, Y.; Yao, L.; Jian, Z. Crystallization Kinetics of the $Fe_{68}Nb_6B_{23}Mo_3$ Glassy Ribbons Studied by Differential Scanning Calorimetry. *Crystals* **2022**, *12*, 852. https://doi.org/10.3390/cryst12060852.
21. Zhang, L.I.; Yu, P.F.; Cheng, H.; Zhang, M.D.; Liu, D.J.; Zhou, Z.; Jin, Q.; Liaw, P.K.; Li, G.; Liu, R.P. Crystallization in Fe- and Co-based amorphous alloys studied by in-situ X-ray diffraction. *Metallurgical and Materials Transactions A* **2016**, *47*. https://doi.org/10.1007/s11661-016-3761-7.
22. Zhu, J.S.; Wang, Y.G.; Xia, G.T.; Dai, J.; Chen, J.K. $Fe_{83}P_{14.5}Cu_1Al_{1.5}$ partial nanocrystalline alloy obtained by one-step melt spinning method. *Journal of Alloys and Compound* **2016**, *666*. https://dx.doi.org/10.1016/j.jalcom.2016.01.055.
23. Li, G.; Li, D.; Ni, X.; Li, Z.; Lu, Z. Effect of copper and niobium addition on crystallization kinetics in Fe-Cu-Nb-Si-B alloys. Rare *Metal Materials and Engineering* **2013**, *42(7)*, 1352-1355. https://doi.org/10.1016/51875-5372(13)60084-3.
24. Malow, T.R.; Koch,C.C. Grain growth in nanocrystalline iron prepared by mechanical attrition. *Acta Materialia* **1997**, *45(5)*, 2197-2186. https://doi.org/10.1016/S1359-6454(96)00300-X.
25. Wu, X.; Li, X.; Li, S. Crystallization kinetics and soft magnetic properties of $Fe_{71}Si_{16}B_9Cu_1Nb_3$ amorphous alloys. *Materials Research Express* **2020**, *7*, 016118. https://doi.org/10.1088/2053-1591/ab6c89.
26. Liu, Y.J.; Chang, I.T.H.; Lees, M.R. Thermodynamic and magnetic properties of multicomponent $(Fe,Ni)_{70}Zr_{10}B_{20}$ amorphous alloy powders made by mechanical alloying. *Materials Science and Engineering A* **2001**, *304-306*, 992-996. https://doi.org/10.1016/S0921-5093(00)01613-0.
27. Manchanda, B.; Vimal, K.K.; Kapur, G.S.; Kant, S.; Choudhary, V. Effect of sepiolite on nonisothermal crystallization kinetics of polypropylene. *Journal of Materials Science* **2016**, *51*, 9535-9550. https://doi.org/10.1007/s10853-016-0210-3.
28. Gao, Q.; Jian, Z. Kinetic study on non-isothermal crystallization of $Cu_{50}Zr_{50}$ metallic glass. *Trans Indian Inst Mat.* **2017**, *70(7)*. https://doi.org.10.1007/s12666-016-0992-7.
29. Hasani, S.; Rezaei-Shahreza, P.; Seifoddini, A. The effect of Cu minor addition on the non-isothermal kinetic of nano-crystallites formation in $Fe_{41}Co_7Cr_{15}Mo_{14}Y_2C_{15}B_6$ BMG. *Journal of Thermal Analysis and Calorimetry* **2021**, *143(5)*. https://doi.org/10.1007/s10973-020-09716-6.
30. Jaafari, Z.; Seifoddini, A.; Hasani, S.; Rezaei-Shahreza, P. Kinetic analysis of crystallization process in $[(Fe_{0.9}Ni_{0.1})_{(77)}Mo_5P_9C_{7.5}B_{1.5}]_{(100-x)}Cu_x$ (x=0.1at.%) BMG: Non-isothermal condition. *Journal of Thermal Analysis and Calorimetry* **2018**, *134(3)*, 1565-1574. https:/doi.org/10.1007/s10973-018-7372-y.
31. Janovsky, D.; Sveda, M.; Sycheva, A.; Kristaly, F.; Zamborsky, F.; Koziel, T.; Bala, P.; Czel, G.; Kaptay, G. Amorphous alloys and differential scanning calorimetry (DSC). *Journal of Thermal Analysis and Calorimetry* **2022**, *147*, 7141-7157. https://doi.org/10.1007/s10973-021-11054-0.
32. Kaloshkin, S.; Churyukanova, M.; Tcherdyntsev, V. Characterization of Magnetic Transformation at Curie Temperature in Finemet-type Microwires by DSC. *MRS Online Proceedings Library* **2012**, *1408*, 107-112. https://doi.org/10.1557/opl.2012.2.
33. Alleg, S.; Brahimi, A.; Azzaza, S.; Souilah, S.; Zergoug, M.; Suñol, J.J.; Greneche, J.M. X-ray diffraction, Mössbauer spectroscopy and thermal studies of the mechanically alloyed $(Fe_{1-x}Mn_x)_2P$ powders. *Advanced Powder Technology* **2018**, *29(2)*, 257-265. https://doi.org/10.1016/j.apt.2017.11.009.
34. González A.; Bonastre A.; Escoda L.; Suñol JJ. Thermal analysis of Fe(Co,Ni) based alloys prepared by mechanical alloying. 2007. *Journal of Thermal Analysis and Calorimetry* **2007**, *87*, 255-258. https://doi.org/10.1007/s10973-006-7802-0.
35. Neamtu, B.V.; Chicinas, H.F.; Gabor, M.; Marinca, T.F.; Lupu, N.; Chicinas, I. A comparative of the Fe-based amorphous alloy prepared by mechanical alloying and rapid quenching. *J Alloys & Comp.* **2017**, *703*, 19-25. https://doi.org/10.1016/j.jalcom.2017.01.359.

 doi:10.20944/preprints202304.1172.v1

disclaim responsibility for any injury to people or property resulting from any ideas, methods, instructions or products referred to in the content.